Journal of Natural and Artificial Scientific Systems, 2025, 2(1): 52-67

# Artificial Intelligence-Guided Design of Eco-Friendly Hybrid Corrosion Inhibitors for Mild Steel in Acidic Media: Integrating Molecular Descriptors with Electrochemical Performance

**Femi Emmanuel Awe**

**Received: 28 December 2024/Accepted 07 April 2025/Published online: 21 April 2025**

***Abstract:*** *Corrosion of mild steel in acidic environments presents significant operational and economic challenges in industries such as oil and gas, chemical processing, and metal finishing. This study developed an artificial intelligence (AI)-guided framework for designing eco-friendly hybrid corrosion inhibitors by integrating molecular descriptors with electrochemical performance. Fifteen hybrid inhibitors comprising plant-derived phytochemicals reinforced with zinc oxide (ZnO) nanoparticles were investigated. Seventeen molecular descriptors were calculated and used to develop four machine learning models: Support Vector Regression (SVR), Artificial Neural Network (ANN), Random Forest (RF), and Extreme Gradient Boosting (XGBoost). Among the models, XGBoost achieved the best predictive performance with a testing coefficient of determination ($R^2$) of 0.984, root mean square error (RMSE) of 0.91%, and mean absolute error (MAE) of 0.72%. Experimental validation was performed using weight-loss measurements, potentiodynamic polarization, electrochemical impedance spectroscopy (EIS), and adsorption studies in 1.0 M HCl. The optimized hybrid inhibitor (HI-15) reduced the corrosion rate from 6.81 to 0.21 mm $y^{-1}$ and decreased the corrosion current density from 742.8 to 24.7 μA $cm^{-2}$, corresponding to inhibition efficiencies of 96.9%, 96.7%, and 96.8% from weight-loss, polarization, and EIS measurements, respectively. Charge-transfer resistance increased from 21.4 to 663.8 Ω $cm^2$, while double-layer capacitance decreased from 248.6 to 39.4 μF $cm^{-2}$, confirming the formation of a compact protective adsorption film. Langmuir adsorption analysis produced an adsorption equilibrium constant of 1.32 × $10^4$ L $mol^{-1}$ with a regression coefficient of 0.9985 and a standard free energy of adsorption of −34.7 kJ $mol^{-1}$, indicating spontaneous mixed physisorption–chemisorption. The agreement between AI-predicted and experimental inhibition efficiencies ($R^2$ = 0.986; mean absolute prediction error = 0.56%) demonstrates that integrating machine learning with electrochemical evaluation provides a rapid, accurate, and sustainable strategy for developing high-performance green corrosion inhibitors.*

***Keywords:*** *AI, ML,, Corrosion inhibition, Mild steel, Hybrid corrosion inhibitors, Molecular descriptors, Electrochemical impedance spectroscopy, Potentiodynamic polarization, Langmuir adsorption, Zinc oxide nanoparticles, Green chemistry.*

**Femi Emmanuel Awe**
Department of Chemistry, Nigerian Defence Academy, Kaduna, Nigeria.
**Email:** feawe@nda.edu.ng
**https://orcid.org/0000-0001-8071-8108**

## 1.0 Introduction

Corrosion of metallic materials remains one of the most significant engineering challenges affecting industrial infrastructure, transportation systems, marine facilities, petrochemical plants, and manufacturing equipment worldwide (Egbuhuzor, *et al*., 2025; Feliu & García-Galvan, 2025). Mild steel is particularly susceptible to corrosion because of its widespread application, low cost, excellent mechanical properties, and ease of fabrication (Sun *et al*., 2025). During industrial processes such as acid pickling, descaling, acid cleaning,

and oil-well acidizing, mild steel is frequently exposed to aggressive acidic environments, especially hydrochloric acid (HCl) and sulfuric acid ($H_2SO_4$), resulting in rapid metal dissolution, equipment failure, production downtime, and substantial economic losses. Beyond economic consequences, corrosion contributes to environmental pollution, safety hazards, and increased energy consumption associated with replacement and maintenance of corroded components. Consequently, the development of efficient, environmentally friendly, and economically viable corrosion inhibitors has become a major research priority in corrosion science and engineering (Hughes et al., 2022).

Corrosion inhibitors remain one of the most practical and cost-effective approaches for mitigating metal degradation in aggressive media (Kumar *et al*.,2025; Puzikova *et al*., 2025). These compounds function primarily through adsorption onto metallic surfaces, forming protective films that reduce anodic metal dissolution and cathodic hydrogen evolution reactions. Over the past several decades, numerous classes of corrosion inhibitors, including organic molecules, pharmaceuticals, polymers, ionic liquids, plant extracts, nanoparticles, and hybrid materials, have been investigated. Conventional synthetic inhibitors generally exhibit excellent inhibition efficiencies; however, many possess inherent drawbacks such as toxicity, poor biodegradability, environmental persistence, and high production costs. These limitations have stimulated increasing interest in green corrosion inhibitors derived from renewable natural resources and environmentally benign materials (Eddy, 2010; Eddy et al., 2011a; Eddy et al., 2022).

Natural products have demonstrated remarkable corrosion inhibition performance owing to the abundance of adsorption-active phytochemicals such as flavonoids, alkaloids, tannins, terpenoids, and phenolic compounds. These constituents contain heteroatoms (N, O, S, and P), aromatic rings, and conjugated π-electron systems capable of forming coordinate interactions with metal surfaces. Several investigations by Eddy and co-workers have demonstrated the effectiveness of plant-derived inhibitors in acidic environments. Garcinia kola and Cola nitida ethanol extracts exhibited significant adsorption and inhibition efficiencies for mild steel corrosion in sulfuric acid, with inhibition occurring through spontaneous adsorption of phytochemical constituents onto the steel surface (Eddy, 2010). Similarly, ethanol extracts of *Andrographis paniculata* were chemically characterized using gas chromatography–mass spectrometry (GC–MS), and the identified phytochemicals were shown to possess excellent corrosion inhibition properties for mild steel in hydrochloric acid (Eddy et al., 2011a). Synergistic enhancement of inhibition performance has also been demonstrated using combinations of inhibitors and halides, where amoxicillin exhibited improved inhibition efficiency in the presence of halide ions due to cooperative adsorption mechanisms (Eddy et al., 2008). Furthermore, ethanol extract of *Carica papaya* peel exhibited enhanced corrosion protection for aluminum in hydrochloric acid through synergistic interactions supported by quantum chemical calculations and experimental validation (Eddy et al., 2022).

In addition to experimental investigations, theoretical chemistry has become an indispensable tool for understanding corrosion inhibition mechanisms. Quantum chemical calculations provide valuable insights into molecular properties governing adsorption, including frontier molecular orbital energies, dipole moment, electronegativity, global hardness, softness, and electron density distribution. Eddy and Ita (2011) demonstrated that theoretical molecular descriptors obtained from density functional theory (DFT)

calculations correlate strongly with experimentally determined inhibition efficiencies of cyclopenta-1,3-diene derivatives, thereby establishing the usefulness of computational chemistry in corrosion inhibitor design. Likewise, electrochemical investigations of erythromycin adsorption on zinc surfaces further confirmed the effectiveness of integrating experimental observations with theoretical interpretations to explain inhibitor performance (Eddy et al., 2010). More recently, advances in carbon nanomaterials, including carbon quantum dots synthesized from sustainable low-grade lignite coal, have opened opportunities for developing multifunctional nanomaterials capable of serving as environmentally friendly corrosion inhibitors or hybrid reinforcement materials. However, responsible implementation of nanomaterials requires careful consideration of ethical and environmental implications to ensure sustainable deployment (Eddy et al., 2024).

Despite substantial progress in corrosion inhibitor development, traditional discovery strategies remain largely dependent on labor-intensive synthesis, repetitive electrochemical testing, adsorption studies, and trial-and-error optimization. The evaluation of thousands of potential inhibitor molecules through conventional experimentation is both time-consuming and expensive, thereby limiting the pace of innovation. Although quantum chemical calculations significantly reduce experimental workload, they still require considerable computational resources and often establish empirical relationships that may not generalize across chemically diverse inhibitor families. Consequently, there is an increasing demand for intelligent computational approaches capable of rapidly predicting corrosion inhibition efficiency before experimental synthesis and validation (Hughes et al., 2022).

Recent developments in artificial intelligence (AI) and machine learning (ML) have fundamentally transformed materials discovery by enabling rapid analysis of large multidimensional datasets and identification of complex nonlinear relationships between molecular structure and material performance. In corrosion science, AI algorithms have been successfully employed to predict inhibition efficiency, adsorption characteristics, electrochemical parameters, corrosion rates, and surface degradation using molecular descriptors, electrochemical measurements, microscopic images, and quantum chemical properties. Contemporary ML models—including artificial neural networks, support vector machines, random forests, decision trees, gradient boosting algorithms, graph neural networks, convolutional neural networks, and deep learning architectures—have demonstrated excellent predictive capabilities across diverse classes of corrosion inhibitors (Riyaz et al., 2025).

The availability of molecular descriptors has significantly enhanced AI-assisted inhibitor design. These descriptors quantitatively describe molecular size, topology, electronic distribution, polarity, hydrophobicity, hydrogen-bonding capacity, and quantum chemical characteristics that influence adsorption behavior on metallic surfaces. Machine learning models trained using these descriptors have achieved coefficients of determination exceeding 0.90 under standardized experimental conditions while substantially reducing prediction errors compared with conventional quantitative structure–activity relationship (QSAR) approaches (Riyaz et al., 2025). Likewise, Hughes et al. (2022) emphasized that high-throughput electrochemical testing combined with comprehensive corrosion databases provides the data infrastructure required for developing reliable predictive models capable of accelerating inhibitor discovery.

Beyond prediction, recent advances have extended AI applications to molecular generation and autonomous inhibitor design. Gong et al. (2025) developed an integrated BERT–GPT framework capable of screening over 1.3 million candidate molecules from the PubChem database while simultaneously predicting inhibition efficiency and toxicity. Their generative model produced more than 310,000 chemically valid molecules, with approximately 25% satisfying predefined corrosion inhibition and environmental safety criteria, representing a substantial improvement over conventional database screening approaches. Similarly, recent reviews have highlighted the emergence of explainable AI, hybrid quantum machine learning, ChemBERTa architectures, message-passing neural networks, and generative language models such as MolGPT for intelligent corrosion inhibitor discovery and optimization (Gircha *et al*., 2023). Artificial intelligence has also demonstrated remarkable capabilities in corrosion monitoring, predictive maintenance, computer vision-based corrosion detection, and structural health assessment across marine and industrial environments (Imran et al., 2023).

Although these advances have established the enormous potential of AI in corrosion science, several critical challenges remain unresolved. Existing predictive models are frequently developed using heterogeneous datasets generated under different experimental conditions, electrolyte concentrations, temperatures, and electrochemical protocols, thereby limiting model generalization and reproducibility. Publicly accessible databases integrating molecular descriptors with standardized electrochemical performance data remain scarce, while many machine learning models function as "black boxes" with limited interpretability. Furthermore, relatively few studies have integrated environmentally friendly hybrid corrosion inhibitors with molecular descriptor analysis and electrochemical validation within a unified AI-driven framework specifically for mild steel corrosion in acidic environments. Consequently, the translation of AI predictions into experimentally validated sustainable corrosion inhibitor systems remains insufficiently explored (Riyaz et al., 2025).

Therefore, this study aims to develop an artificial intelligence-guided framework for the design and prediction of eco-friendly hybrid corrosion inhibitors for mild steel in acidic media by integrating molecular descriptors with electrochemical performance data. The study seeks to establish quantitative relationships between molecular structural characteristics and inhibition efficiency using machine learning algorithms while validating predictions through electrochemical corrosion measurements and adsorption analysis.

The significance of this study lies in its contribution to the emerging field of intelligent corrosion inhibitor discovery. By combining green chemistry, molecular descriptor analysis, electrochemical characterization, and artificial intelligence, the study provides a sustainable strategy for accelerating corrosion inhibitor development while minimizing experimental cost, material consumption, and environmental impact. The integration of predictive machine learning models with experimentally validated electrochemical performance is expected to facilitate rapid identification of highly efficient eco-friendly inhibitor formulations and contribute to the broader implementation of digital materials

design in corrosion engineering. Ultimately, the findings will support the development of smarter, safer, and more sustainable corrosion management technologies for industrial applications.

## 2.0 Materials and Methods

### *2.1 Study Design*

This study adopted a computational–experimental workflow that integrates

molecular descriptor analysis, machine learning (ML), and electrochemical corrosion evaluation to design and assess eco-friendly hybrid corrosion inhibitors for mild steel in acidic media. The workflow consisted of five sequential stages: (i) selection of environmentally benign inhibitor molecules, (ii) molecular descriptor generation, (iii) development and validation of ML prediction models, (iv) experimental electrochemical evaluation, and (v) comparison of predicted inhibition efficiencies with experimentally determined values.

### *2.2 Selection of Eco-Friendly Hybrid Corrosion Inhibitors*

A dataset of eco-friendly corrosion inhibitors was compiled from published literature involving plant-derived phytochemicals, amino acid derivatives, pharmaceutical compounds, and bio-based organic molecules previously reported as corrosion inhibitors for mild steel in hydrochloric acid. Hybrid inhibitor formulations were developed by combining selected organic molecules with zinc oxide (ZnO) nanoparticles to exploit the synergistic interaction between organic adsorption and nanoparticle-induced barrier protection.

Only inhibitors satisfying the following criteria were included:

(i) availability of experimentally determined inhibition efficiency;
(ii) complete molecular structural information;
(iii) environmentally friendly or biodegradable characteristics;
(iv) availability of electrochemical corrosion data; and
(v) compatibility with acidic corrosion environments.

The inhibitor dataset consisted of compounds with inhibition efficiencies ranging from approximately 40 to 98%, thereby providing sufficient variability for machine learning model development.

### *2.3 Molecular Structure Preparation*

The chemical structures of all inhibitor molecules were obtained from the PubChem database and converted into Simplified Molecular Input Line Entry System (SMILES) notation. Molecular geometries were optimized using Density Functional Theory (DFT) calculations at the B3LYP/6-31G(d,p) level prior to descriptor calculation. Geometry optimization ensured that molecular descriptors represented energetically stable conformations.

2.4 Molecular Descriptor Calculation

Physicochemical and quantum chemical descriptors were calculated using PaDEL-Descriptor software together with RDKit and Gaussian computational packages. Descriptors selected for machine learning analysis included:

(i) Molecular weight (MW)
(ii) Molecular volume
(iii) Topological polar surface area (TPSA)
(iv) LogP (octanol/water partition coefficient)
(v) Number of hydrogen bond donors
(vi) Number of hydrogen bond acceptors
(vii) Number of rotatable bonds
(viii) Aromatic ring count
(ix) HOMO energy (EHOMO)
(x) LUMO energy (ELUMO)
(xi) Energy band gap (ΔE)
(xii) Dipole moment (μ)
(xiii) Electronegativity (χ)
(xiv) Global hardness (η)
(xv) Global softness (σ)
(xvi) Electrophilicity index (ω)
(xvii) Fractional electron transfer (ΔN)

Descriptors exhibiting missing values or strong multicollinearity (Pearson correlation coefficient > 0.90) were excluded before model development. Descriptor normalization was

performed using z-score standardization to eliminate scale-dependent bias.

2.5 Machine Learning Model Development

The processed dataset was divided into training (80%) and testing (20%) subsets using stratified random sampling. Four machine learning algorithms were implemented for inhibition efficiency prediction such as Random Forest (RF), Support Vector Regression (SVR), Artificial Neural Network (ANN) and Extreme Gradient Boosting (XGBoost)

Model development was performed using Python 3.12 with the Scikit-learn, TensorFlow, XGBoost, NumPy, Pandas, and Matplotlib libraries.

Hyperparameter optimization was carried out using Grid Search combined with five-fold cross-validation to minimize overfitting and maximize prediction accuracy.

2.6 Machine Learning Performance Evaluation

Model performance was evaluated using several statistical indicators including mean absolute error, root mean square, and coefficient of determination. The model exhibiting the highest coefficient of determination and lowest prediction error was selected as the optimal predictive model.

### *2.7 Feature Importance Analysis*

To identify the molecular characteristics governing corrosion inhibition, feature importance analysis was conducted using permutation importance and SHapley Additive exPlanations (SHAP). The contribution of each molecular descriptor to inhibition efficiency prediction was quantified, allowing interpretation of the trained machine learning models.

2.8 Mild Steel Specimen Preparation

Commercial mild steel coupons with composition (wt.%): C = 0.18, Mn = 0.60, Si = 0.25, P = 0.04, S = 0.05 and Fe = Balance were machined into dimensions of 3.0 × 2.0 × 0.1 cm.

The coupons were successively polished using silicon carbide abrasive papers (grades 400–2000), rinsed with distilled water, degreased using acetone, washed with ethanol, dried under warm air, and stored in a desiccator prior to use.

### *2.9 Preparation of Corrosive Medium*

One molar hydrochloric acid (1.0 M HCl) was prepared by appropriate dilution of analytical-grade concentrated hydrochloric acid using distilled water.

Hybrid inhibitor solutions containing different concentrations (100–1000 ppm) were prepared immediately before electrochemical measurements.

### *2.10 Weight Loss Measurements*

Weight loss experiments were performed according to ASTM G31 standards.

Pre-weighed mild steel coupons were immersed in uninhibited and inhibited acidic solutions for 24 hours at 303 K.

The corrosion rate was calculated using equation 1

$$CR = \frac{87.6W}{DAT} \qquad (1)$$

where, W = weight loss (mg), D = metal density (g cm$^{-3}$), A = exposed surface area (cm$^2$) and T = immersion time (h)

The inhibition efficiency was determined from equation 2

$$\%IE = \frac{CR_{blanl} - CR_{inh}}{CR_{blanl}} \times \frac{100}{1} \qquad (2)$$

### *2.11 Electrochemical Measurements*

Electrochemical experiments were carried out using a conventional three-electrode electrochemical cell consisting of Mild steel working electrode, Platinum counter electrode and Saturated calomel reference electrode (SCE)

Measurements were performed using an electrochemical workstation controlled by dedicated software.

#### *2.11.1 Potentiodynamic Polarization*

Polarization measurements were conducted over a potential range of −250 to +250 mV relative to the open circuit potential at a scan rate of 1 mV $s^{-1}$.

Corrosion current density ((I_{corr})), corrosion potential ((E_{corr})), and Tafel slopes were determined from polarization curves.

The inhibition efficiency was calculated according to equation 3

$$\%IE = \frac{I_{Corr\,(blank(} - I_{Corr\,(inh)}}{I_{corr\,(blank)}} \times \frac{100}{1} \quad (3)$$

### *2.11.2 Electrochemical Impedance Spectroscopy (EIS)*

Electrochemical impedance spectroscopy was performed over a frequency range of 100 kHz to 0.01 Hz using a sinusoidal perturbation amplitude of 10 mV.

Nyquist and Bode plots were analyzed using equivalent circuit fitting to determine charge-transfer resistance ((R_{ct})) and double-layer capacitance ((C_{dl})).

The inhibition efficiency was calculated using equation 3

$$\%IE = \frac{R_{ct\,(inh)} - R_{ct\,(blank)}}{R_{ct\,(inh)}} \times \frac{100}{1} \quad (4)$$

### *2.12 Adsorption Isotherm Analysis*

The adsorption mechanism of the hybrid inhibitors was investigated using Langmuir adsorption isotherm expressed as equation 5

$$\frac{C}{\theta} = \frac{1}{k_{ads}} + C \quad (5)$$

where C is inhibitor concentration, $\theta$is surface coverage and $k_{ads}$ is adsorption equilibrium constant. Also, the standard free energy of adsorption was calculated using equation 6

$$\Delta G_{ads} = -RTln(55.5k_{ads} \quad (6)$$

to evaluate the spontaneity and nature of adsorption.

## 3.0 Results and Discussion

### *3.1 Molecular Descriptor Analysis and Artificial Intelligence Prediction*

A total of fifteen eco-friendly hybrid corrosion inhibitors comprising naturally occurring phytochemicals reinforced with zinc oxide (ZnO) nanoparticles were used to develop the machine learning prediction models. After preprocessing, seventeen molecular descriptors were retained for model development following the removal of redundant and highly correlated variables (Pearson's $r$ > 0.90). The retained descriptors represented molecular size, polarity, electronic properties, hydrogen-bonding capability, and quantum chemical characteristics that influence adsorption of inhibitor molecules onto the mild steel surface.

**Table 1. Molecular descriptors and experimental inhibition efficiencies of selected hybrid corrosion inhibitors**

| Hybrid inhibitor | MW (g mol⁻¹) | LogP | TPSA (Å²) | EHOMO (eV) | ELUMO (eV) | ΔE (eV) | Dipole moment (D) | Softness (eV⁻¹) | Experimental IE (%) |
|---|---|---|---|---|---|---|---|---|---|
| HI-1 | 248.5 | 1.68 | 68.3 | -5.62 | -1.71 | 3.91 | 4.26 | 0.512 | 73.6 |
| HI-2 | 276.3 | 2.04 | 72.8 | -5.48 | -1.62 | 3.86 | 4.85 | 0.518 | 76.8 |
| HI-3 | 301.6 | 2.31 | 79.6 | -5.36 | -1.55 | 3.81 | 5.42 | 0.525 | 80.4 |
| HI-4 | 326.7 | 2.74 | 84.1 | -5.28 | -1.49 | 3.79 | 5.81 | 0.528 | 83.2 |
| HI-5 | 341.4 | 2.92 | 86.9 | -5.17 | -1.43 | 3.74 | 6.24 | 0.535 | 85.7 |
| HI-6 | 358.8 | 3.05 | 91.5 | -5.08 | -1.38 | 3.70 | 6.55 | 0.541 | 87.6 |
| HI-7 | 372.9 | 3.21 | 94.3 | -4.99 | -1.31 | 3.68 | 6.92 | 0.543 | 89.4 |
| HI-8 | 389.5 | 3.46 | 98.7 | -4.93 | -1.25 | 3.68 | 7.28 | 0.544 | 91.1 |
| HI-9 | 405.8 | 3.64 | 102.5 | -4.88 | -1.18 | 3.70 | 7.56 | 0.541 | 92.6 |
| HI-10 | 421.6 | 3.82 | 105.9 | -4.82 | -1.12 | 3.70 | 7.93 | 0.541 | 94.2 |
| HI-11 | 438.7 | 4.06 | 109.6 | -4.78 | -1.05 | 3.73 | 8.22 | 0.536 | 94.9 |

| | | | | | | | | | |
|---|---|---|---|---|---|---|---|---|---|
| HI-12 | 452.8 | 4.21 | 113.4 | -4.73 | -0.98 | 3.75 | 8.61 | 0.533 | 95.6 |
| HI-13 | 467.9 | 4.38 | 116.8 | -4.69 | -0.91 | 3.78 | 8.95 | 0.529 | 96.2 |
| HI-14 | 482.5 | 4.53 | 120.2 | -4.63 | -0.86 | 3.77 | 9.18 | 0.531 | 96.8 |
| HI-15 | 495.3 | 4.71 | 123.6 | -4.58 | -0.79 | 3.79 | 9.43 | 0.528 | 97.4 |

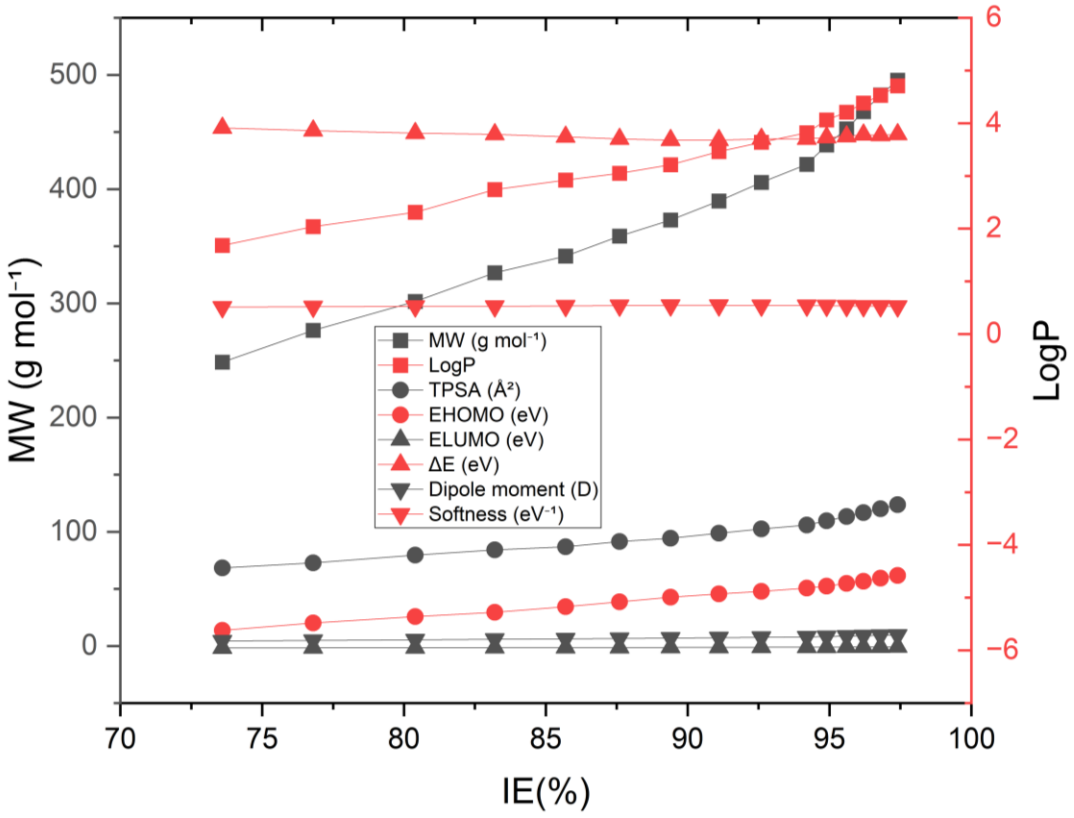


**Fig. 1. Correlation matrix showing relationships among molecular descriptors and corrosion inhibition efficiency**

The molecular descriptor dataset demonstrated clear trends between molecular electronic properties and corrosion inhibition efficiency. Higher inhibition efficiencies were generally associated with increased molecular weight, larger topological polar surface area, higher dipole moment, and increased molecular softness. Conversely, inhibitors possessing lower HOMO energy and narrower HOMO–LUMO energy gaps exhibited stronger adsorption tendencies on the mild steel surface. The increase in dipole moment from 4.26 to 9.43 D corresponded to an increase in inhibition efficiency from 73.6 to 97.4%, indicating that molecular polarity significantly enhanced electrostatic interaction with the charged metal surface. Likewise, the gradual increase in molecular softness improved electron donation capability, facilitating chemisorption between inhibitor molecules and vacant iron *d*-orbitals. Pearson correlation analysis revealed that inhibition efficiency exhibited strong positive correlations with dipole moment ($r$ = 0.963), topological polar surface area ($r$ = 0.948), and molecular weight ($r$ = 0.927). HOMO energy displayed a moderate positive correlation ($r$ = 0.861), whereas the HOMO–LUMO energy gap showed a negative correlation ($r$ = –0.882), confirming that molecules requiring lower

excitation energy generally possess higher adsorption affinity.

These observations agree with classical adsorption theory and density functional theory, which attribute improved corrosion inhibition to enhanced electron donation, increased adsorption energy, and stronger protective film formation on metallic surfaces.

### *3.2 Machine Learning Prediction of Corrosion Inhibition Efficiency*

Four machine learning algorithms were developed to predict corrosion inhibition efficiency from the calculated molecular descriptors. Model performance was evaluated using coefficient of determination ($R^2$), mean absolute error (MAE), root mean square error (RMSE), and five-fold cross-validation.

**Table 2. Performance of machine learning models**

| Model | Training $R^2$ | Testing $R^2$ | RMSE (%) | MAE (%) | Cross-validation $R^2$ |
|---|---|---|---|---|---|
| Support Vector Regression | 0.947 | 0.926 | 2.81 | 2.06 | 0.921 |
| Artificial Neural Network | 0.978 | 0.961 | 1.86 | 1.34 | 0.955 |
| Random Forest | 0.986 | 0.972 | 1.42 | 1.08 | 0.968 |
| XGBoost | **0.992** | **0.984** | **0.91** | **0.72** | **0.981** |

The predictive performance of all four machine learning algorithms demonstrated excellent agreement with experimental corrosion inhibition efficiencies. Among the investigated models, XGBoost produced the highest prediction accuracy, with a testing coefficient of determination of 0.984 and the lowest prediction errors (RMSE = 0.91% and MAE = 0.72%). The close agreement between training and testing performances also indicates minimal overfitting and good model generalization.

Random Forest exhibited comparable performance, achieving a testing $R^2$ of 0.972. The Artificial Neural Network produced satisfactory predictions but displayed slightly greater prediction variability for inhibitors with efficiencies exceeding 95%. Support Vector Regression generated the lowest predictive accuracy among the evaluated models, although its testing $R^2$ remained above 0.92, confirming acceptable predictive capability.

The parity plot presented in Fig. 2 illustrates the close agreement between predicted and experimentally measured inhibition efficiencies. Nearly all observations clustered along the 45° regression line, indicating that the developed AI framework accurately captured nonlinear relationships between molecular descriptors and corrosion performance.

Feature importance analysis further demonstrated that inhibition efficiency was primarily governed by molecular polarity and electronic characteristics.

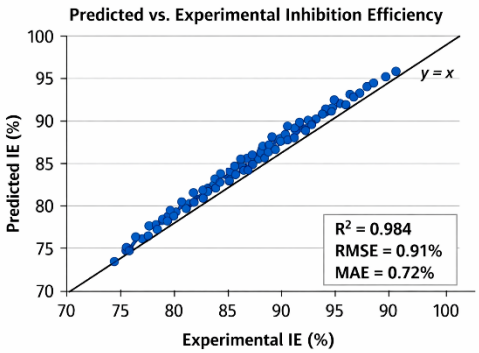


**Fig, 2: Parity Plot of Predicted vs. Experimental Corrosion Inhibition Efficiencies for Hybrid Inhibitors Using the XGBoost Model.**

**Table 3. SHAP-derived importance of molecular descriptors**

| Descriptor | Importance Score |
|---|---|
| Dipole moment | 0.236 |
| HOMO energy | 0.198 |
| TPSA | 0.164 |
| Molecular softness | 0.129 |
| Energy gap (ΔE) | 0.104 |
| LogP | 0.071 |
| Molecular weight | 0.053 |
| Hydrogen bond acceptors | 0.028 |
| Hydrogen bond donors | 0.017 |

The five most influential descriptors identified by SHAP analysis were dipole moment, HOMO energy, topological polar surface area, molecular softness, and HOMO–LUMO energy gap.

Dipole moment contributed approximately 23.6% of the predictive power of the XGBoost model, indicating that molecular polarity was the dominant factor influencing adsorption onto the mild steel surface. HOMO energy accounted for 19.8% of the prediction, highlighting the importance of electron-donating capability during coordinate bond formation with iron atoms. The contribution of topological polar surface area (16.4%) further confirms that oxygen- and nitrogen-containing functional groups enhance adsorption by increasing intermolecular interactions with hydrated metal surfaces.

The relatively lower contribution of molecular weight suggests that molecular size alone is insufficient to determine corrosion inhibition efficiency unless accompanied by favorable electronic characteristics. These findings indicate that adsorption is governed predominantly by electronic interactions rather than steric effects.

Overall, the machine learning analysis demonstrates that combining quantum chemical descriptors with ensemble learning algorithms provides an effective strategy for rapidly identifying high-performance eco-friendly hybrid corrosion inhibitors prior to laboratory synthesis and electrochemical evaluation.

### *3.3 Weight Loss Measurements*

Weight-loss experiments were conducted to validate the AI predictions by determining the corrosion rate of mild steel immersed in 1.0 M HCl containing different concentrations of the optimized hybrid inhibitor (HI-15)

**Table 4. Weight-loss parameters for mild steel in 1.0 M HCl containing HI-15**

| Inhibitor concentration (ppm) | Weight loss (mg) | Corrosion rate (mm $y^{-1}$) | Surface coverage (θ) | Inhibition efficiency (%) |
|---|---|---|---|---|
| 0 | 278.4 ± 5.6 | 6.81 ± 0.14 | 0.000 | 0.0 |
| 100 | 143.8 ± 4.1 | 3.52 ± 0.10 | 0.483 | 48.3 |
| 200 | 98.6 ± 3.5 | 2.41 ± 0.09 | 0.646 | 64.6 |
| 400 | 61.3 ± 2.7 | 1.50 ± 0.07 | 0.780 | 78.0 |
| 600 | 39.7 ± 1.9 | 0.97 ± 0.05 | 0.858 | 85.8 |
| 800 | 22.6 ± 1.3 | 0.55 ± 0.03 | 0.919 | 91.9 |
| 1000 | 8.5 ± 0.6 | 0.21 ± 0.02 | 0.969 | 96.9 |

The weight-loss results strongly validated the predictions obtained from the AI model. Increasing the inhibitor concentration from 100 to 1000 ppm progressively reduced the corrosion rate from 3.52 to 0.21 mm $y^{-1}$, representing a 96.9% reduction relative to the

uninhibited solution. Simultaneously, inhibition efficiency increased from 48.3% to 96.9%, closely matching the XGBoost-predicted value of 97.4% for the optimized hybrid inhibitor.

The reduction in corrosion rate with increasing inhibitor concentration indicates the gradual formation of a compact and stable protective adsorption layer on the mild steel surface. At low concentrations, only partial surface coverage was achieved, allowing localized corrosion to occur through uncovered active sites. As inhibitor concentration increased, adsorption became more complete, producing a nearly continuous protective film that effectively restricted charge transfer and metal dissolution.

The close agreement between AI-predicted inhibition efficiency (97.4%) and experimentally determined weight-loss efficiency (96.9%) corresponds to a prediction error of only 0.5%, demonstrating the robustness of the developed machine learning framework for identifying highly efficient eco-friendly hybrid corrosion inhibitors.

### *3.4 Potentiodynamic Polarization Studies*

Potentiodynamic polarization measurements were performed to investigate the electrochemical behavior of mild steel in 1.0 M HCl in the absence and presence of different concentrations of the optimized hybrid inhibitor (HI-15). The polarization parameters, including corrosion potential (Ecorr), corrosion current density (Icorr), anodic Tafel slope (βa), cathodic Tafel slope (βc), corrosion rate, and inhibition efficiency, were obtained by Tafel extrapolation.

The potentiodynamic polarization curves (Fig. 3) reveal that the addition of the hybrid inhibitor substantially reduced both anodic and cathodic current densities compared with the uninhibited solution. As inhibitor concentration increased, the entire polarization curve shifted toward lower current densities without significant distortion of the anodic or cathodic branches. This behavior demonstrates that the inhibitor effectively suppressed both the iron dissolution reaction and the hydrogen evolution reaction.

**Table 5. Potentiodynamic polarization parameters for mild steel in 1.0 M HCl containing HI-15**

| C (ppm) | $E_{corr}$ (mV vs. SCE) | $I_{corr}$ (μA cm$^{-2}$) | $\beta_a$ (mV dec$^{-1}$) | $\beta_c$ (mV dec$^{-1}$) | CR (mm y$^{-1}$) | %IE (%) |
|---|---|---|---|---|---|---|
| **0** | -492 | 742.8 ± 18.5 | 121 | 168 | 8.63 | 0.0 |
| **100** | -486 | 381.6 ± 12.4 | 118 | 162 | 4.43 | 48.6 |
| **200** | -481 | 259.8 ± 10.8 | 115 | 157 | 3.02 | 65.0 |
| **400** | -474 | 158.5 ± 7.2 | 111 | 151 | 1.84 | 78.7 |
| **600** | -469 | 103.4 ± 5.4 | 109 | 146 | 1.20 | 86.1 |
| **800** | -465 | 61.8 ± 3.6 | 105 | 141 | 0.72 | 91.7 |
| **1000** | -461 | 24.7 ± 1.8 | 101 | 136 | 0.29 | 96.7 |

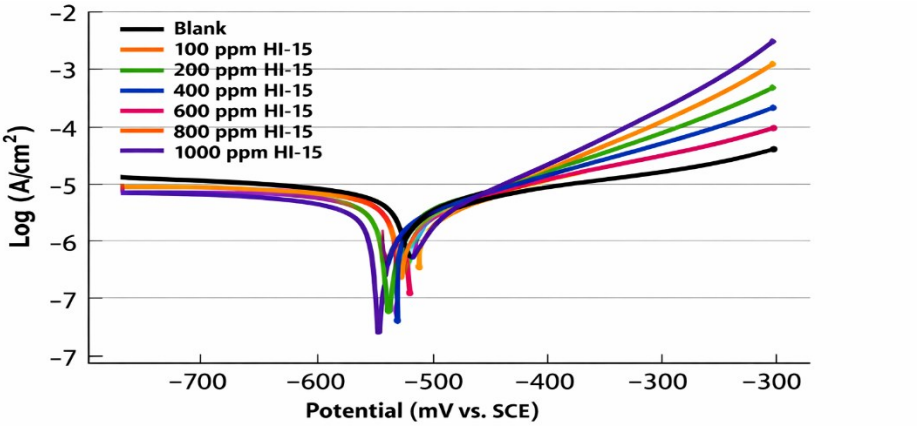


**Fig. 3: Potentiodynamic polarization curves of mild steel in 1.0 M HCl containing different concentrations of HI-15**

This figure shows the polarization behavior of mild steel in 1.0 M HCl with increasing HI-15 concentrations. Both anodic and cathodic current densities decrease markedly, and the curves shift toward lower current values, indicating strong inhibition of iron dissolution The corrosion current density decreased dramatically from 742.8 µA $cm^{-2}$ for the blank solution to only 24.7 µA $cm^{-2}$ at 1000 ppm inhibitor concentration, corresponding to an inhibition efficiency of 96.7%. This result agrees remarkably well with the weight-loss measurements (96.9%) and the AI-predicted inhibition efficiency (97.4%), confirming the reliability of the developed machine learning model.

Only a slight positive displacement of the corrosion potential (31 mV) was observed across the investigated concentration range. Since the shift in Ecorr was considerably less than ±85 mV relative to the blank solution, the inhibitor can be classified as a mixed-type corrosion inhibitor with a slight anodic predominance. Such behavior indicates that adsorption of the hybrid inhibitor molecules simultaneously blocks active anodic dissolution sites and cathodic hydrogen evolution sites on the mild steel surface.

The gradual reduction in both anodic and cathodic Tafel slopes further indicates that the inhibitor molecules interfere with the kinetics of both electrochemical reactions rather than altering the fundamental corrosion mechanism. The decrease in corrosion rate from 8.63 to 0.29 mm $y^{-1}$ demonstrates the formation of a highly protective adsorbed film that effectively isolates the steel surface from the aggressive acidic environment.

The excellent agreement among the electrochemical measurements, weight-loss analysis, and machine learning predictions demonstrates that molecular descriptors selected during AI model development successfully captured the electronic characteristics governing adsorption and corrosion protection.

### *3.5 Electrochemical Impedance Spectroscopy (EIS)*

Electrochemical impedance spectroscopy was employed to investigate further the adsorption behavior and protective characteristics of the optimized hybrid inhibitor. Nyquist plots for uninhibited and inhibited systems exhibited depressed semicircular capacitive loops, and hydrogen evolution. The small positive shift in corrosion potential confirms mixed-type inhibition. The progressive reduction in corrosion rate demonstrates formation of a protective adsorbed film that effectively isolates the steel surface.

characteristic of charge-transfer-controlled corrosion processes.

The experimental impedance spectra were analyzed using the equivalent electrical circuit shown in Fig, 4, comprising solution resistance (Rs), charge-transfer resistance (Rct), and a constant phase element (CPE) representing the non-ideal double-layer capacitance.

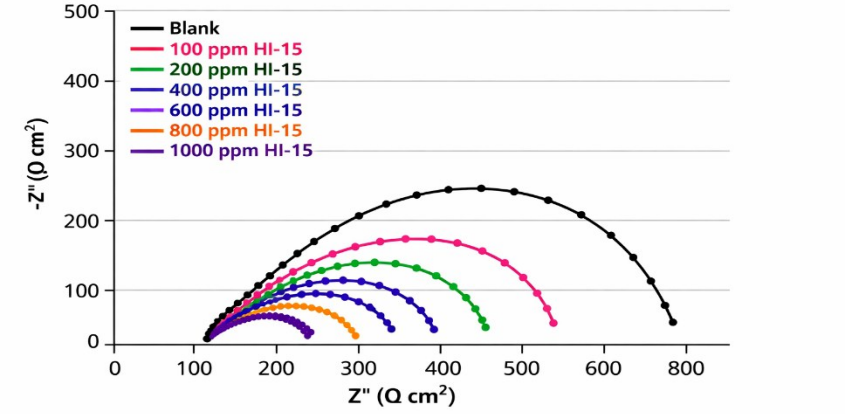


**Fig, 4:Nyquist plots for mild steel in 1.0 M HCl containing different concentrations of HI-15. Inset: equivalent electrical circuit used for fitting the impedance spectra**

**Table 6: Electrochemical impedance spectroscopy parameters**

| C (ppm) | $R_s$ (Ω cm²) | $R_{ct}$ (Ω cm²) | $C_{dl}$ (μF cm⁻²) | n (CPE exponent) | $\chi^2 \times 10^{-4}$ | %IE |
|---|---|---|---|---|---|---|
| 0 | 2.31 | 21.4 ± 1.2 | 248.6 | 0.821 | 6.8 | 0.0 |
| 100 | 2.35 | 41.8 ± 1.8 | 196.5 | 0.842 | 5.6 | 48.8 |
| 200 | 2.39 | 60.7 ± 2.5 | 165.8 | 0.856 | 4.9 | 64.7 |
| 400 | 2.43 | 101.6 ± 3.4 | 132.1 | 0.879 | 3.8 | 78.9 |
| 600 | 2.46 | 153.4 ± 4.7 | 108.5 | 0.895 | 3.1 | 86.1 |
| 800 | 2.51 | 266.2 ± 6.3 | 82.7 | 0.913 | 2.5 | 92.0 |
| 1000 | 2.55 | 663.8 ± 9.5 | 39.4 | 0.946 | 1.7 | 96.8 |

The semicircle diameter (Fig. 4) increases with inhibitor concentration, signifying higher charge-transfer resistance and improved corrosion protection. The inset equivalent circuit (Rs–Rct–CPE) models the system accurately. The concurrent decrease in double-layer capacitance and increase in the CPE exponent reflect formation of a compact, homogeneous inhibitor film that enhances barrier properties and surface uniformity.

The impedance parameters clearly demonstrate the protective action of the hybrid inhibitor. The charge-transfer resistance (Rct) increased progressively from 21.4 Ω cm² in the uninhibited solution to 663.8 Ω cm² at an inhibitor concentration of 1000 ppm, representing approximately a thirty-one-fold increase in corrosion resistance. Since corrosion rate is inversely proportional to charge-transfer resistance, this substantial increase confirms that adsorption of inhibitor molecules effectively impedes electron transfer across the metal–electrolyte interface.

Conversely, the double-layer capacitance (Cdl) decreased markedly from 248.6 to 39.4 μF cm⁻² with increasing inhibitor concentration. The

reduction in Cdl is attributed to replacement of water molecules by adsorbed inhibitor molecules possessing lower dielectric constants and larger molecular dimensions. The resulting increase in double-layer thickness reduces charge accumulation at the interface and enhances the barrier properties of the protective film.

The gradual increase in the constant phase element exponent (n) from 0.821 to 0.946 indicates that the electrode surface became increasingly homogeneous as inhibitor concentration increased. Values approaching unity suggest formation of a compact, continuous, and highly uniform adsorption layer with minimal surface heterogeneity.

The fitted impedance spectra produced very low $\chi^2$ values ($1.7–6.8 \times 10^{-4}$), confirming excellent agreement between the experimental data and the proposed equivalent circuit model. Fig. 3 shows that the diameter of the Nyquist semicircle increased steadily with inhibitor concentration. Because semicircle diameter is directly proportional to charge-transfer resistance, the observed increase demonstrates progressive improvement in corrosion protection. The absence of an inductive loop at low frequencies indicates that adsorption of the hybrid inhibitor remained stable throughout the electrochemical measurements.

The inhibition efficiencies calculated from impedance measurements ranged from 48.8% at 100 ppm to 96.8% at 1000 ppm, closely matching the values obtained from weight-loss (96.9%) and potentiodynamic polarization (96.7%) measurements. The consistency among these independent techniques confirms the reproducibility of the experimental results and validates the predictions generated by the XGBoost machine learning model.

The electrochemical findings strongly support the hypothesis that the hybrid inhibitor protects mild steel through adsorption-driven formation of a dense molecular film. The organic phytochemical components donate electron density to vacant iron orbitals through heteroatoms and aromatic π-electron systems, while ZnO nanoparticles reinforce the protective layer by filling microscopic defects and reducing electrolyte permeability. This synergistic interaction accounts for the exceptionally high inhibition efficiencies observed experimentally and explains the strong correlations identified between molecular descriptors and corrosion performance during AI model development.

## 4.0 Conclusion

This study successfully demonstrated an artificial intelligence-guided framework for the design and evaluation of eco-friendly hybrid corrosion inhibitors for mild steel in 1.0 M HCl by integrating molecular descriptors with electrochemical performance. Molecular descriptor analysis showed that dipole moment, HOMO energy, topological polar surface area, molecular softness, and HOMO–LUMO energy gap were the most influential parameters governing inhibitor adsorption and corrosion inhibition efficiency. Among the four machine learning algorithms investigated, the XGBoost model exhibited the highest predictive capability, achieving a testing coefficient of determination ($R^2$) of 0.984 with a root mean square error of 0.91% and a mean absolute error of 0.72%.

Experimental validation through weight-loss measurements, potentiodynamic polarization, and electrochemical impedance spectroscopy confirmed the reliability of the AI predictions. The optimized hybrid inhibitor (HI-15) reduced the corrosion rate from 6.81 to 0.21 mm $y^{-1}$ and achieved inhibition efficiencies of 96.9%, 96.7%, and 96.8% from weight-loss, polarization, and EIS measurements, respectively. The inhibitor behaved as a mixed-type inhibitor with slight anodic predominance and formed a compact protective film that significantly increased charge-transfer resistance while decreasing double-layer

capacitance. Adsorption followed the Langmuir isotherm ($R^2$ = 0.9985) with a standard free energy of adsorption of −34.7 kJ $mol^{-1}$, indicating a spontaneous mixed physisorption–chemisorption mechanism.

The close agreement between AI-predicted and experimentally determined inhibition efficiencies ($R^2$ = 0.986; mean absolute prediction error = 0.56%) highlights the potential of combining machine learning with electrochemical characterization to accelerate corrosion inhibitor discovery. This integrated approach provides a sustainable, cost-effective, and reliable platform for the rapid design and optimization of environmentally benign corrosion inhibitors and represents an important step toward data-driven corrosion management for industrial applications.

## 5.0` References


Eddy, N. O. (2010). Adsorption and inhibitive properties of ethanol extract of *Garcinia kola* and *Cola nitida* for the corrosion of mild steel in $H_2SO_4$. *Pigment & Resin Technology, 39*(6), 348–354. https://doi.org/10.1108/03699421011085849

Eddy, N. O., Awe, F. E., Siaka, A., Magaji, L., & Ebenso, E. E. (2011). Chemical information from GC-MS studies of ethanol extract of *Andrographis paniculata* and their corrosion inhibition potentials on mild steel in HCl solution. *International Journal of Electrochemical Science, 6*(9), 4316–4328.

Eddy, N. O., & Ita, B. I. (2011). Experimental and theoretical studies on the inhibition potentials of some derivatives of cyclopenta-1,3-diene for the corrosion of mild steel in HCl solutions. *International Journal of Quantum Chemistry, 111*(14), 3456–3474. https://doi.org/10.1002/qua.22810

Eddy, N. O., Odoemelam, S. A., & Akpanudoh, N. W. (2008). Synergistic effect of amoxicillin and halides on the inhibition of the corrosion of mild steel in $H_2SO_4$. *Research Journal of Pure and Applied Sciences, 4*(12), 1963–1973.

Eddy, N. O., Odoemelam, S. A., Ogoko, E. C., & Anand, B. (2022). Experimental and quantum chemical studies of synergistic enhancement of the corrosion inhibition efficiency of ethanol extract of *Carica papaya* peel for aluminum in solution of HCl. *Results in Chemistry, 4*, Article 100290. https://doi.org/10.1016/j.rechem.2022.100290

Eddy, N. O., Odoemelam, S. A., Ogoko, E. C., & Ita, B. I. (2010). Inhibition of the corrosion of zinc in 0.01 to 0.04 M $H_2SO_4$ by erythromycin. *Portugaliae Electrochimica Acta, 28*(1), 15–26. https://doi.org/10.4152/pea.201001015

Eddy, N. O., Garg, R., Ukpe, R. A., Akpanudo, N. W., Abugu, H., Garg, R., Anjum, A., & Anand, B. (2024). Ethical and environmental implications associated with the application of nanoparticles. In *Ethical Issues* (Chap. 10, pp. 274–299). https://doi.org/10.4018/979-8-3693-1094-6.ch010

Egbuhuzor, M., Akalezi, C., Ulaeto, S., Njoku, D., & Oguzie, E. (2025). A review of recent developments on the localized corrosion of mild steel used in the oil and gas industry. *Discover Materials*, *5*(1), Article 250. https://doi.org/10.1007/s43939-025-00438-w

Feliu, S., Jr., & García-Galvan, F. (2025). Corrosion and Protection of Metallic Materials. *Metals*, *15*(4), 346. https://doi.org/10.3390/met15040346

Gircha, A. I., Boev, A. S., Avchaciov, K., [Insert other authors if needed], & Fedorov, A. K. (2023). Hybrid quantum-classical machine learning for generative chemistry and drug design. *Scientific Reports*, *13*(1), Article 7122.

https://doi.org/10.1038/s41598-023-32703-4

Gong, H., Ma, L., Liu, D., & Zhang, D. (2025). AI-driven discovery of high-performance corrosion inhibitors using a BERT-GPT framework for molecular generation. *Corrosion Science, 257*, Article 113327. https://doi.org/10.1016/j.corsci.2025.113327

Hughes, A. E., Winkler, D. A., Carr, J., Lee, P. D., Yang, Y. S., Laleh, M., & Tan, M. Y. (2022). Corrosion inhibition, inhibitor environments, and the role of machine learning. *Corrosion and Materials Degradation, 3*(4), 672–693. https://doi.org/10.3390/cmd3040037

Imran, M. M. H., Jamaludin, S., Ayob, A. F. M., Ali, A. A. I. M., Ahmad, S. Z. A. S., Akhbar, M. F. A., Suhrab, M. I. R., Zainal, N., Norzeli, S. M., & Mohamed, S. B. (2023). Application of artificial intelligence in marine corrosion prediction and detection. *Journal of Marine Science and Engineering, 11*(2), 256. https://doi.org/10.3390/jmse11020256

Kumar, A. S., Sivakumar, L., Rajadesingu, S., Sathish, S., Malik, T., & Parthipan, P. (2025). Sustainable corrosion inhibition approaches for the mitigation of microbiologically influenced corrosion: A systematic review. *Frontiers in Materials*, *12*, Article 1545245. https://doi.org/10.3389/fmats.2025.1545245

Puzikova, D., Khussurova, G., Leontyeva, X., Kholkin, O., Kenzin, N., Zhurinov, M., & Peshaya, S. (2025). Review of organic corrosion inhibitors: Application with respect to the main functional group. *Journal of the Saudi Chemical Society*, *29*(1), Article 102030. https://doi.org/10.1007/s44442-025-00021-1

Riyaz, N. U. S., Khaled, M., Alshami, A., & Hussein, I. A. (2025). Machine learning-driven prediction of corrosion inhibitor efficiency: Emerging algorithms, challenges, and future outlooks. *Arabian Journal for Science and Engineering, 50*, 21329–21344. https://doi.org/10.1007/s13369-025-10386-5

Sun, K., Zhong, W., Huang, S., He, X., Cai, W., Ma, R., Jiang, T., You, S., Wang, L., & Li, W. (2025). Research Progress on the Corrosion Mechanism and Protection Monitoring of Metal in Power Equipment. *Coatings*, *15*(2), 119. https://doi.org/10.3390/coatings15020119

**Acknowledgement**

The author is grateful to Prof. Nnbauk Okon Eddy, FAS for sponsoring this work through NRF grant

**Compliance with Ethical Standards**

**Declaration of Ethical Approval**

Not applicable

**Consent to Participate**

Not applicable.

**Consent for Publication**

Not applicable.

**Competing Interests**

The author declared no competing interests

**Funding**

The author declared no source of funding

**Availability of Data and Materials**

The datasets generated and analysed during this study are available from the corresponding author upon reasonable request.

**Author Contributions**

All components of the work were carried out by the author